Water Science & Technology

Water Science & Technology Vol 88 No 11, 2849 doi: 10.2166/wst.2023.391

High performance of membrane capacitive deionization with ZnS/g-C_3N_4 composite electrodes

Shiyu Wei[a,b], Ling Feng[a], Xuliu Zhang[a], Zhumei Sun[a], Hongjuan Bai[a] and Pengxiao Liu[a,*]

[a] School of Environment and Safety Engineering, North University of China, Taiyuan 030051, China
[b] Shanxi Coking Coal Group Co., Ltd, Taiyuan 030051, China
*Corresponding author. E-mail: lpx@nuc.edu.cn

PL, 0000-0002-2968-6742

ABSTRACT

Capacitive deionization (CDI) is considered a promising technology for desalination of sea or brackish water. In this study, a ZnS/g-C_3N_4 composite was synthesized through a one-step high-temperature method and used as the main material to fabricate CDI electrodes. The results of SEM and TEM showed that spherical-like nanoparticles of ZnS were uniformly distributed on the g-C_3N_4 sheet. The g-C_3N_4 phase facilitates the ZnS particles precipitate and restrain their agglomeration, which contributes to a high specific surface area of ZnS. Furthermore, the electrochemical test results indicated that ZnS/g-C_3N_4 composite had a good capacitance characteristic, low resistance, and high electrochemical stability. Finally, the desalinization performance of the ZnS/g-C_3N_4 composite electrodes was tested in traditional mode and membrane capacitive deionization (MCDI) mode. The results showed that ZnS/g-C_3N_4//ZnS/g-C_3N_4 (MCDI) exhibited an optimal desalination capacity. The adsorption amount was 27.65, 50.26, and 65.34 mg/g for NaCl initial concentration of 200, 400, and 600 mg/L, respectively, with the voltage of 1.2 V and flow rate of 5 mL/min. Increasing initial concentration enhanced the conductivity and ion migration rate so as to increase the NaCl adsorption amount. ZnS/g-C_3N_4 composite can be used as potential electrode material for high performance of MCDI.

Key words: capacitive deionization, electrode materials, g-C_3N_4, ZnS

HIGHLIGHTS

- Capacitive deionization (CDI) has emerged as a promising approach to desalination.
- ZnS/g-C_3N_4 composite can be used for CDI.
- ZnS/g-C_3N_4 has a large specific surface area.
- ZnS/g-C_3N_4 showed a high desalination capacity of 65.34 mg/g in membrane capacitance deionization (MCDI).

GRAPHICAL ABSTRACT

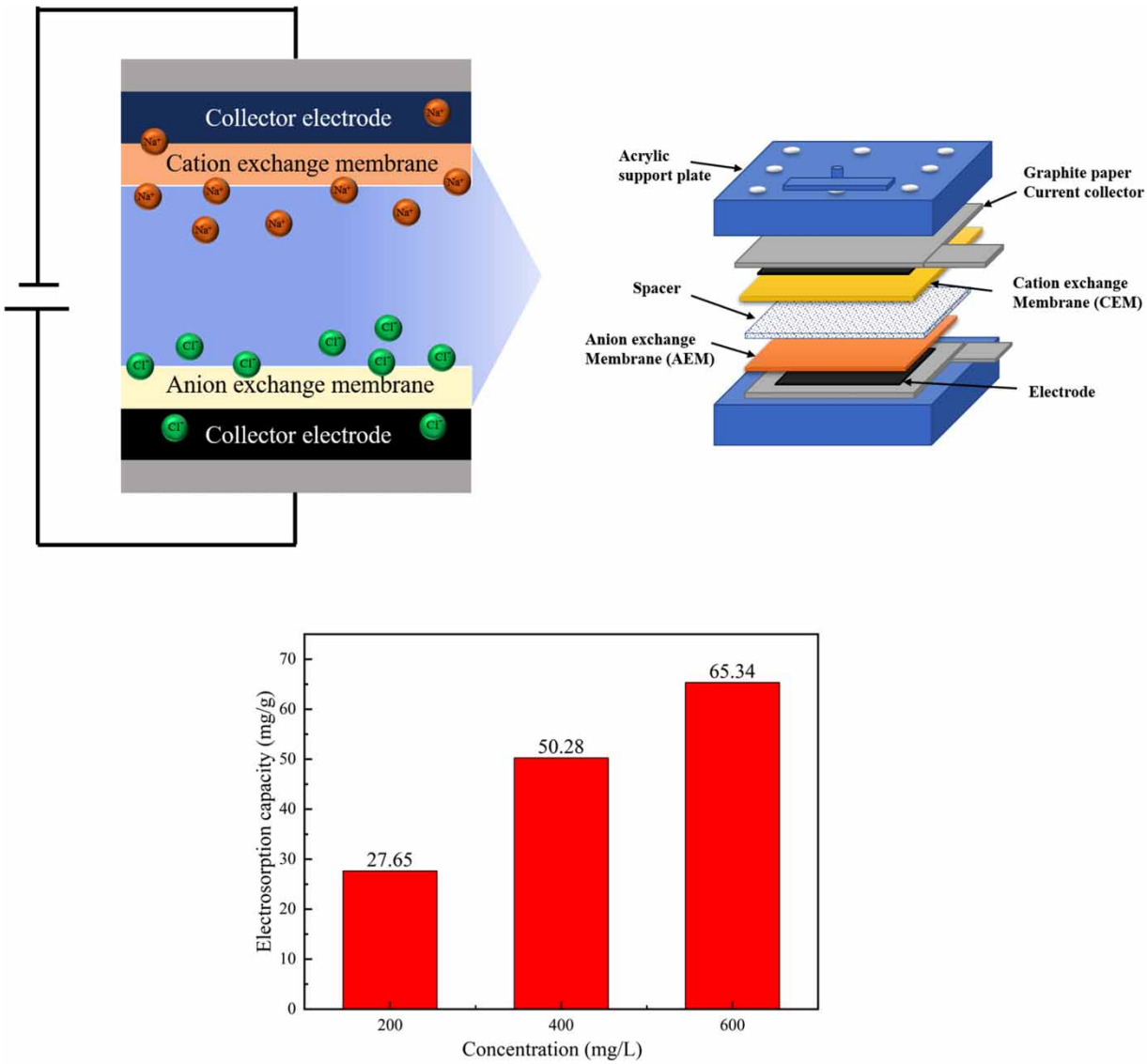

INTRODUCTION

With the development of industry and the growth of population, the global demand for freshwater is rapidly increasing, and the original scarce freshwater resources are more tense. Since seawater and brackish water account for more than 96% of total water resources on the earth (Shiklomanov 2000), obtaining fresh water from seawater or micro-salt water has attracted considerable attention, which is supposed to be a feasible strategy to relieve the crisis of fresh water shortage. Traditional desalination technologies, such as reverse osmosis, multi-stage flash distillation, and electrodialysis processes have showed the disadvantages of excessive energy consumption, high cost, and low efficiency, which hinders their more widespread application (Mohamed *et al.* 2020). New desalination techniques that are energy efficient and cost-effective are explored all the time.

Capacitive deionization (CDI) technology has been a research hotspot in the area of seawater or brackish water desalination in recent years (Chung *et al.* 2020; Torkamanzadeh *et al.* 2020; Gong *et al.* 2021), which shows the advantages of low energy consumption, ecological friendliness, high separation, simple design, and easy operation (Yan *et al.* 2018). The technique is simple and easy to operate. Desalting can be carried out at low pressure and room temperature, and the applied

voltage at both ends of the electrode generally does not exceed 1.6 V. Unlike reverse osmosis or distillation-based desalination systems, CDI does not need to be coupled to a high-pressure pump or heat source, allowing easy system scaling (Suss *et al.* 2015). Additionally, CDI is environmentally favorable because energy, rather than chemicals, is used to power the operation process. Therefore, it does not cause secondary pollution to water bodies, and is a clean and efficient desalination technology. This is mostly a physical process that allows CDI equipment to have a long service life and low maintenance costs (Porada *et al.* 2013). During the desalination process, saline ions are attracted and stored in the electrical double layer of charged electrodes, and released from the surface of discharged electrodes. Electrode material is crucial for the performance of CDI as its structure, porosity, surface and electrochemical properties greatly determine the ions adsorption efficiency (Peng *et al.* 2011; Dlugolecki & van der Wal 2013). Carbon materials, such as activated carbon, mesoporous carbon, carbon nanotubes, carbon aerogels, and graphene are mainly used for CDI electrode preparation because of the large surface area and wide pore size distribution (Huang *et al.* 2017; Leong *et al.* 2019). However, drawbacks of low conductivity, irregular pore shape and size distribution of these carbon-based electrodes limit the CDI desalination capacity (Sufiani *et al.* 2019). Therefore, exploring new electrode materials for high performance of the CDI system are necessary.

The graphite phase carbon nitride (g-C_3N_4) is a novel non-metallic semiconductor material with the merit of environment friendly large specific surface area, good electrical conductivity, etc. (Zheng *et al.* 2012). g-C_3N_4 has caused broad interest in the scientific community as photocatalyst. Also, it is begun to be used as electrode active materials in recent years due to its good conductivity and hydrophilicity. For example, Wang *et al.* (2018) used g-C_3N_4 as electrode materials for CDI, showing an excellent salt adsorption capacity and cyclic stability. Kavil *et al.* (2018) prepared nano-g-C_3N_4/MnO_2 and g-C_3N_4/SnO_2 composites for supercapacitor applications, and the g-C_3N_4 improved the specific surface area and promoted the electron transport at the electrode-electrolyte interface. Thiagarajan *et al.* (2020) prepared $NiMoO_4$/g-C_3N_4 for supercapacitors, which showed a large specific capacitance (501 F/g) and high stability, maintaining a capacity of up to 91.8% even after 2,000 charge and discharge cycles. In a word, g-C_3N_4 as electrode materials could improve the conductivity, hydrophilicity, and ion transmission of the electrodes.

Metal sulfides (MSs) are a kind of potential electrode materials in the metal matrix. MSs tend to cause sulfur defects in the formation process, thus forming a large number of active sites, which facilitate the catalytic reaction (Shiraz *et al.* 2021). Zinc sulfide (ZnS) has attracted extensive attention due to its advantages such as high capacity and density, rich sulfur and zinc resources, low cost and less pollution, and has become a cathode material for high performance of energy storage (Guo *et al.* 2018; Xie *et al.* 2018). In addition, ZnS is an important semiconductor material with wide energy gap (3.5–3.8 eV) and high specific capacitance (926.3 mAh/g) (Du *et al.* 2017; Xu *et al.* 2018). However, disadvantages of ZnS, such as poor conductivity and volume expansion have been found as well during its application. Recombination with other materials is supposed to be a way to make up for the deficiency. For example, Sarma *et al.* (2015) synthesized a flower-shaped ZnS/TiO_2 nanotubes composite electrode, showing high specific capacitance and stability under large charging conditions.

In this study, g-C_3N_4 was used as the carrier to support ZnS nanoparticles, and ZnS/g-C_3N_4 composite was prepared by a high-temperature calcination method. The morphology and structure of the composite was analyzed, and the electrode was prepared. The electrochemical characteristics of the composite and the desalination performance were studied. The results show that ZnS can form a spherical particle structure on g-C_3N_4 lamellar layer, which weakens the stacking effect between the carbon nitrification lamellar layer and improves the capacitance of the material, thus improving the capacitive deionization performance of the electrode. The power supply voltage, inflow velocity and initial concentration of NaCl solution all have an effect on the desalting capacity of the capacitor. Through different CDI and MCDI mode tests, ZnS/g-C_3N_4// ZnS/g-C_3N_4 (MCDI) maximum adsorption capacity is 27.65 mg/g.

METHODS

Preparation of g-C_3N_4

Thiourea was chosen as the experimental precursor. To ensure a well-mixed product, 5 g of thiourea was weighed in a mortar and ground for 30 min. After that, it was placed in a quartz boat and then into a tubular furnace (SK-G08123K, Tianjin Zhonghuan Electric Furnace Co., Ltd, China). It was heated to 550 °C at 10 °C/min in a nitrogen atmosphere for 2 h. The light yellow g-C_3N_4 powder was successfully prepared after being cooled to room temperature.

Preparation of ZnS/g-C_3N_4

The precursor of choice was thiourea. To create a homogenous mixture, 1 g of zinc acetate and 5 g of thiourea were weighed and mortared for 30 min. The quartz boat of the tubular furnace should then be used. It was heated to 550 °C under nitrogen environment at a rate of 10 °C/min and maintained for 2 h. To obtain orange ZnS/g-C_3N_4 powder, the mixture was cooled to room temperature.

Preparation of ZnS/g-C_3N_4 electrode

First, ZnS/g-C_3N_4 complex, acetylene black, and polyvinylidene fluoride were ground evenly in a mortar with a mass ratio of 8:1:1. Acetylene black was used as conductive agent and polyvinylidene fluoride was used as adhesive. Then drop N-methyl pyrrolidone as a solvent, stirring for more than half an hour, to obtain an uniform slurry. Using graphite paper as fluid collector, the electrode paste was coated on graphite paper by a simple coating method, and the electrode was obtained by drying it in a drying oven at 60 °C for 12 h.

Material characterization

The microstructure and morphology of the samples were investigated by scanning electron microscopy (SEM, Zeiss MERLIN Compact) and transmission electron microscopy (TEM, FEITecnai G2 F30). X-ray diffractometer (XRD, Rigaku Ultima IV) was used to analyze the crystal structure of the material. Fourier transform infrared spectrometer (FTIR) was used to analyze the structure of the materials, mainly used to determine the surface functional groups of the samples. Nitrogen adsorption and desorption isotherms were measured at 77 K. Before the measurement, the samples were degassed at 463 K for 6 h in vacuum using the McAsap2460 instrument. The Brunauer–Emmett–Teller (BET) method was used to calculate the specific surface area and pore volume. A Barrett–Joyner–Halenda (BJH) model was used to derive the pore size distribution from the adsorption branch of the isotherm. The water contact angle was measured using JY-82C Kruss DSA on the powder sample after compression. Titration of ultrapure water was done automatically using equipment containing 1.6 μL of water droplets.

Electrochemical measurement

In this experiment, electrochemical workstation (CHI660E, Chenhua, China) was used to test the electrochemical performance of samples with a three-electrode system. In 1-M NaCl aqueous solution, a three-electrode system was used at room temperature. g-C_3N_4 and ZnS/g-C_3N_4 composites were used as working electrodes. Before the electrochemical performance test, the working electrodes were immersed in NaCl for 12 h to fully soak the electrolyte solution. Platinum (Pt) electrode and saturated calomel electrode (SCE) were used as the counter electrode and reference electrode, respectively.

The potentials measured by cyclic voltammetry (CV) ranged from −0.2 to 0.8 V at different scanning rates (5, 10, 20, 50, and 100 mv/s). The specific capacitance is obtained from Equation (1). Electrochemical impedance spectroscopy (EIS) was performed in the frequency range of 10^{-2}–10^5 Hz at ac voltage near equilibrium potential (0 V). The test range of constant current charge-discharge (GCD) is −0.2–0.8 V, and the curves of constant current charge–discharge under different current densities (0.2, 0.5, 0.8, 1, 2 A/g) are tested simultaneously.

$$C = \frac{\int I \mathrm{d}V}{2.m \cdot \upsilon \cdot \Delta V} \tag{1}$$

where C is the specific capacitance (F/g), V is the voltage (V), I is the response current (A), V is the scanning rate (V/s), and m refers to the mass of the active substance at the electrode (g).

The specific discharge capacity of the electrode during constant current charge-discharge measurement is calculated according to Equation (2):

$$C_g = \frac{I_m \times \Delta t}{\Delta V} \tag{2}$$

where C_g is the capacitance (F/g), I_m is the current density (A/g), $\triangle t$ is discharge time (s), $\triangle V$ is the discharge potential change (V) without iR drop.

Electrosorption measurement

This CDI experiment was conducted using a self-assembled MCDI module, the operation of which is depicted in Figure 1(a) and the structure schematic diagram in Figure 1(b). The desalination experiments were carried out in 50 mL NaCl solution in an intermittent manner. A conductivity meter, a water storage device, a peristaltic pump, a CDI cell, and a DC stabilized power supply are all part of the system. The self-assembled MCDI module was made up of a Plexiglas spacer, a rubber septum spacer, a pair of parallel electrodes, and a non-woven septum. The electrodes in this experiment were 5cm × 5 cm in size, and a pair of anion and cation exchange membranes were placed in front of the electrode. HoAM G-1204 anion exchange membrane was placed in front of the positive electrode and HoCM G-0014 cation exchange membrane was placed in front of the negative electrode.

The CDI cell operates in flow mode, which means that two electrodes are parallel to each other with a gap between them, allowing brine to flow between them. The NaCl solution was directly driven up and down by a peristaltic pump (BT100-2J, Chinese long pump). The solution entered the device through the lower port and exited through the upper port. The electric field was powered by a constant voltage DC power supply (VICTOR 3003A, China). A conductivity meter was used to continuously record the change in conductivity of the NaCl solution (DDSJ-308F, INESA Scientific Instrument Co. Ltd, China). The concentration of NaCl solution was calculated using the measured conductivity and a standard conductivity-concentration curve.

In this experiment, NaCl solutions of various concentrations were prepared using ultrapure water with conductivity values below 3 μS/cm. At a steady temperature, the conductivity and salt solution concentration have a positive relationship. Supplementary material, Figure S1 depicts the connection between conductivity and the concentration of NaCl solution. By using linear fitting, it was possible to derive the function relationship between solution concentration and conductivity value as $y = 1.9375x + 19.226$ with correlation coefficient $R^2 = 0.9997$, which is a satisfactory fit. It was discovered that, in the solution concentration range of 0–2,000 mg/L, the concentration of NaCl solution showed a good linear association with the

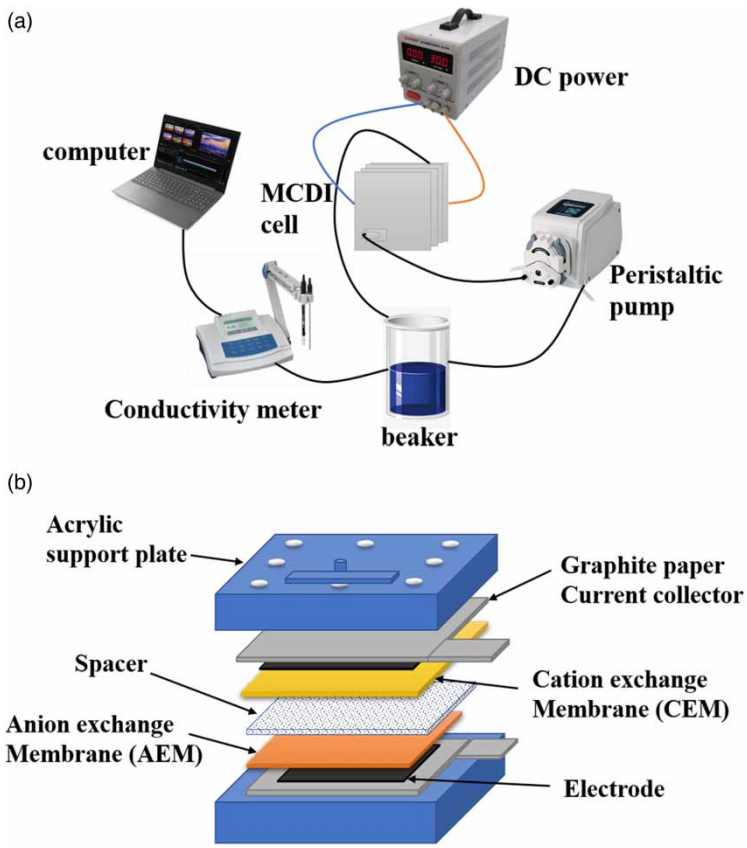

Figure 1 | The schematic diagram of capacitor deionizing process (a) and MCDI cell structure (b).

conductivity. The results of the solution's measured conductivity can be used to determine how much desalination is required given changes in the solution's concentration.

The initial concentration of NaCl was 200 mg/L and the flow rate was 5 mL/min. The desalination performance of g-C_3N_4//g-C_3N_4(CDI), g-C_3N_4//g-C_3N_4(MCDI), ZnS/g-C_3N_4//ZnS/g-C_3N_4(CDI), ZnS/g-C_3N_4//ZnS/g-C_3N_4 (MCDI) was tested at a voltage of 1.2 V. The desorption was performed by short-circuit (voltage 0 V), and the desorption time was 3,500 s. MCDI tests the desalting performance at different flow rates, voltages and initial concentrations are discussed below. Calculate the desalting amount according Equation (3).

$$Q = \frac{C_0 - C_e V_t}{m} \tag{3}$$

where Q is the amount of desalinization, represents the mass of solution ions adsorbed by active substance per gram (mg/g), C_0 and C_e are the initial concentration and adsorption saturation concentration of solution (mg/L) respectively, V_t is the volume of solution (ml), and m is the mass of active substance at the electrode (g).

RESULTS AND DISCUSSION

Structure and composition of ZnS/g-C_3N_4

The morphology of g-C_3N_4 and ZnS/g-C_3N_4 composites was characterized by SEM and TEM. Supplementary material, Figure S2(a) and (b) shows that the pure g-C_3N_4 has a porous and layered stack structure with smooth surfaces. From the SEM images of ZnS/g-C_3N_4 composites (Supplementary material, Figure S2(c) and (d)), it can be observed that spherical-like nanoparticles of ZnS were uniformly distributed on the g-C_3N_4 sheet, and this was further verified by TEM images (Supplementary material, Figure S2(e) and (f)). The g-C_3N_4 phase facilitates the ZnS particles precipitate and restrain their agglomeration, which contributes to a high specific surface area of ZnS. Besides, the porous structure of the composites could be beneficial to the ions diffusion during the desalination process.

Supplementary material (Figure S3) shows the XRD patterns of pure g-C_3N_4 and ZnS/g-C_3N_4 composites. For g-C_3N_4, a weak peak at 13.1° and a strong peak at 27.4° are observed, which correspond to (100) and (002) planes of g-C_3N_4 crystal, respectively (JCPDS No. 87-1526) (Liao *et al.* 2012). For ZnS/g-C_3N_4 composites, there are four additional diffraction peaks at approximately 28.5°, 33.1°, 47.5°, and 56.3°, corresponding to (111), (200), (220), and (311) planes of the hexagonal crystal of ZnS (JCPDS No. 05-0566). The observed diffraction peaks of both g-C_3N_4 and ZnS confirmed the successful synthesis of the ZnS/g-C_3N_4 composite.

The FTIR spectra of g-C_3N_4 and ZnS/g-C_3N_4 composites are shown in Supplementary material, Figure S4. On the g-C_3N_4 curve, the wide absorption peak at 1,243–1,636 cm^{-1} represents the specific stretching mode of C-N heterocyclic ring, and the peak at 808 cm^{-1} may be attributed to the classical stretching mode of triazine units (Zhang *et al.* 2013). In addition, broadband in the range of 3,000–3,500 cm^{-1} shows the elastic oscillation modes of water molecules on the N–H and O–H outer surfaces. The ZnS/g-C_3N_4 composite has similar spectra with pure g-C_3N_4, indicating that ZnS has no significant effect on the structure of g-C_3N_4.

The N_2 adsorption–desorption isotherms and pore size distribution of g-C_3N_4 and ZnS/g-C_3N_4 composites are shown in Figure 2. According to the International Union of Pure and Applied Chemistry's (IUPAC) physical adsorption isotherm classification, ZnS/g-C_3N_4 is a typical type IV adsorption curve with a 'S' shape and a clear H3 hysteresis loop between relative pressures of 0.4 and 0.6, as shown in Figure 2(a). The ZnS/g-C_3N_4 composite appears to have a mesoporous structure and is relatively irregular. The pore size distribution of the ZnS/g-C_3N_4 composite is primarily at 3–4 nm, as shown in Figure 2(b). This is consistent with the isotherm, and the sample does contain pores in the mesoporous region. Mesopores are very important for ion transfer and contribute to ion transport and adsorption properties, as well as improving desalination capacity. The specific surface area, pore volume, and pore size of the materials are shown in Table 1. The specific surface areas of g-C_3N_4 and ZnS/g-C_3N_4 are 6.91 and 10.36 m^2/g, respectively. The spacing effect of the ZnS particles between the g-C_3N_4 layers allows more ions to interact with the material, resulting in improved desalination performance.

The performance of CDI is significantly influenced by the electrode material's wettability, which can be determined using contact angle testing. Supplementary material, Figure S5 illustrates the contact angles of g-C_3N_4 and ZnS/g-C_3N_4 with water. The contact angle is typically less than 90° for hydrophilic materials and more than 90° for hydrophobic ones. Contact angles of 51.37° for g-C_3N_4 and 49.55° for ZnS/g-C_3N_4 show that both substances are hydrophilic. Furthermore, the composite was

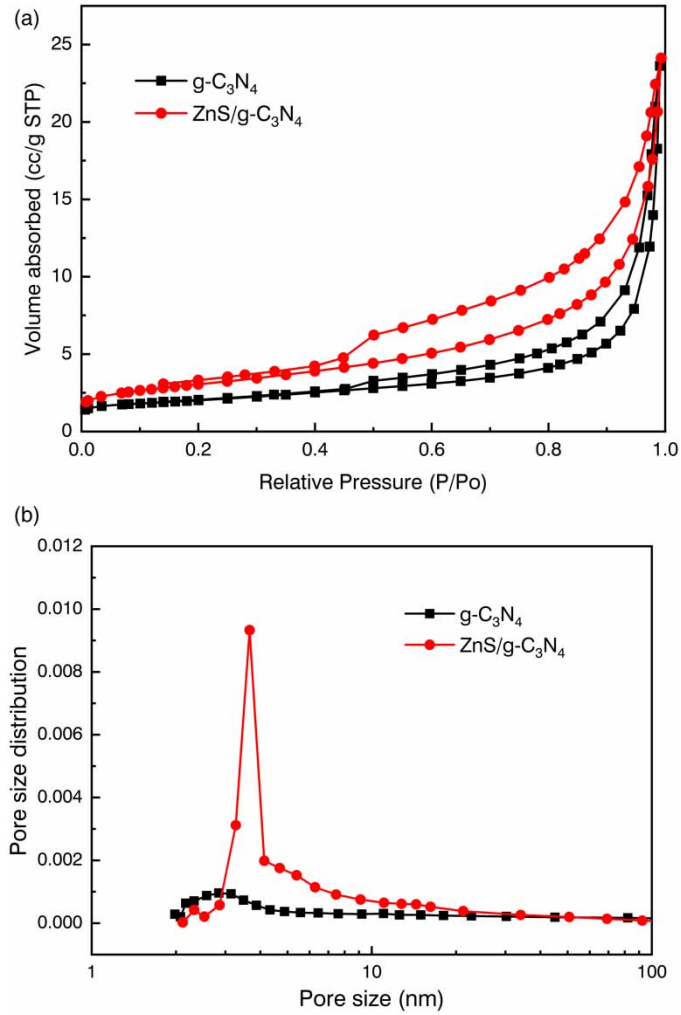

Figure 2 | N_2 adsorption–desorption isotherms (a) and BJH pore size distribution of g-C_3N_4 and ZnS/g-C_3N_4 composites (b).

Table 1 | Characterization of specific surface area, pore volume, and pore size of g-C_3N_4 and ZnS/g-C_3N_4 composites

Sample	S_{BET} (m^2/g)	D (nm)	V_{total} (m^3/g)
g-C_3N_4	6.91	21.16	0.036
ZnS/g-C_3N_4	10.36	14.85	0.037

Note: S_{BET}: special surface area calculated from the BET method; D: average pore diameter; V_{total}: total pore volume.

successfully constructed, increasing its wettability, as evidenced by the decrease in the ZnS/g-C_3N_4 contact angle. The performance of the desalination process is improved by encouraging contact between the NaCl solution and the electrode.

Electrochemical performance of ZnS/g-C_3N_4

The electrochemical properties of g-C_3N_4 and ZnS/g-C_3N_4 were tested in a three-electrode system using 1-M NaCl solution as electrolyte. As shown in Figure 3(a) and 3(b), CV curves of g-C_3N_4 and ZnS/g-C_3N_4 electrodes show good rectangular shapes without redox peaks, indicating that the electrodes have good EDL capacitive characteristics. The rectangular area of ZnS/g-C_3N_4 electrode increases with the increasing scanning rate. The specific capacitance was calculated the specific capacitance of g-C_3N_4 and ZnS/g-C_3N_4 are 24.66 and 30.27 F/g calculated according to Equation (1) at the scanning rate

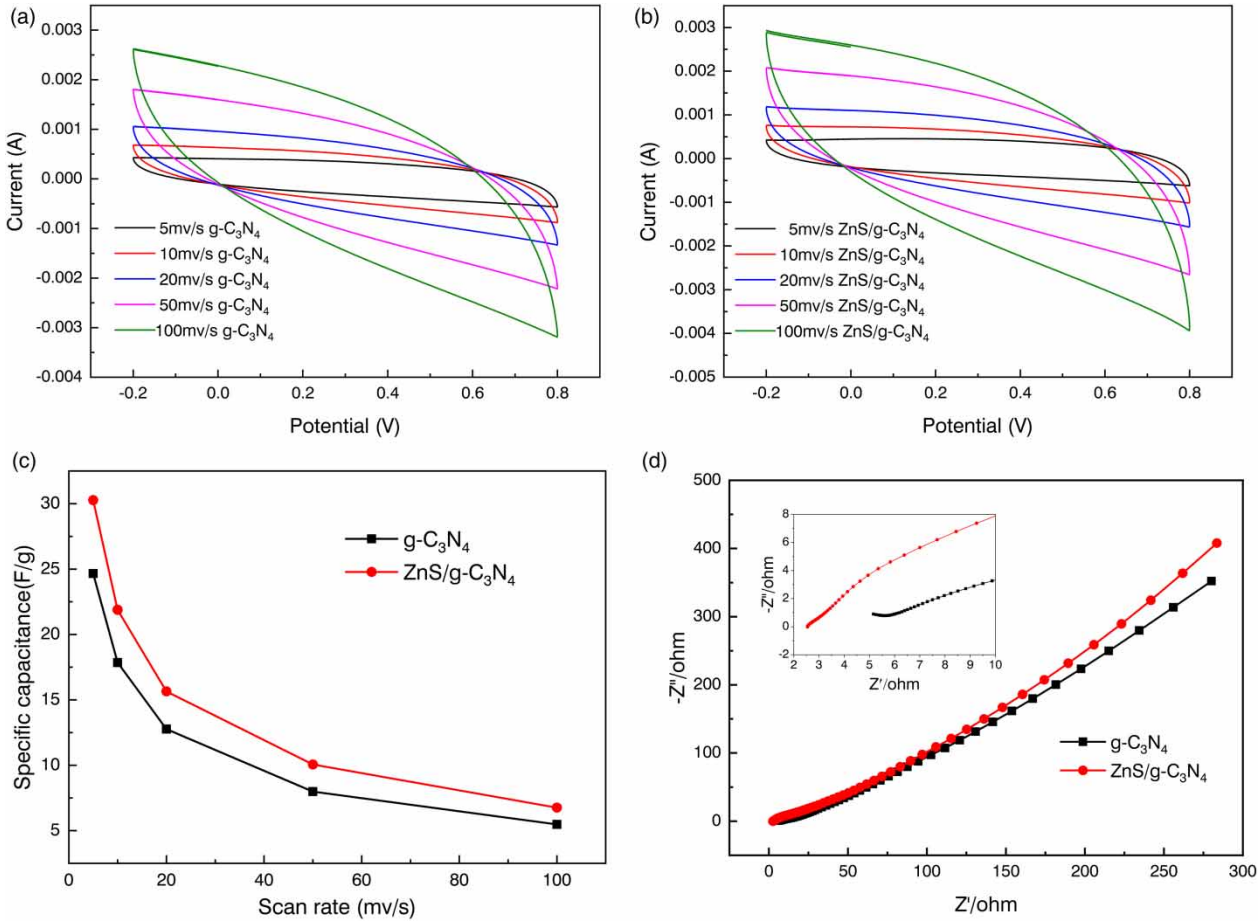

Figure 3 | CV curves of the g-C_3N_4 (a) and ZnS/g-C_3N_4 (b) composite electrode at various scan rates (a), specific capacitances (c), and Nyquist impedance plots (d) for the g-C_3N_4 and ZnS/g-C_3N_4 composite electrodes.

of 5 mV/s. As shown in Figure 3(c), with the increase of scanning rate, the specific capacitance of ZnS/g-C_3N_4 is always higher than that of g-C_3N_4, indicating a better capacitance characteristic.

The EIS test was employed to evaluate the electrical resistance and results are shown in Figure 3(d). ZnS/g-C_3N_4 composite electrode showed a smaller charge transfer resistance. In addition, the slope in the low frequency part of the ZnS/g-C_3N_4 composite electrode is higher than that of g-C_3N_4, suggesting better ion diffusion.

GCD curves of g-C_3N_4 and ZnS/g-C_3N_4 electrodes were measured at different current densities (0.2, 0.5, 0.8, 1, 2 A/g). As shown in Figure 4(a), compared with g-C_3N_4 electrode, the curve of ZnS/g-C_3N_4 electrode presents a longer discharge time, indicating a better conductivity. In addition, the GCD curve of ZnS/g-C_3N_4 electrode has a symmetrical and triangular shape at different current densities, suggesting the capacitance behavior of EDL, which is consistent with the CV curve. The corresponding specific capacitance at different current densities is shown in Figure 4(b). The ZnS/g-C_3N_4 electrode has a higher value than the g-C_3N_4 electrode at any current density.

Desalination performance of ZnS/g-C_3N_4 composite electrodes

Table 2 depicts the electrodes' desalination performance in various modes with an initial concentration of 200 mg/L NaCl solution, a flow rate of 5 mL/min, and a voltage of 1.2 V. The adsorption capacities of the g-C_3N_4//g-C_3N_4 (CDI), ZnS/g-C_3N_4//ZnS/g-C_3N_4 (CDI), g-C_3N_4//g-C3N4 (MCDI) and ZnS/g-C_3N_4///ZnS/g-C_3N_4 (MCDI) processes had adsorption capacities of 4.61, 8.38, 11.05, and 27.65 mg/g, respectively. The best desalination performance was achieved with the ZnS/g-C_3N_4 composite electrode in MCDI mode. It is clear that the use of membranes increases the electrode's adsorption capacity. The use of a membrane during the adsorption process can suppress the co-ion effect and allow the adsorbed ions to

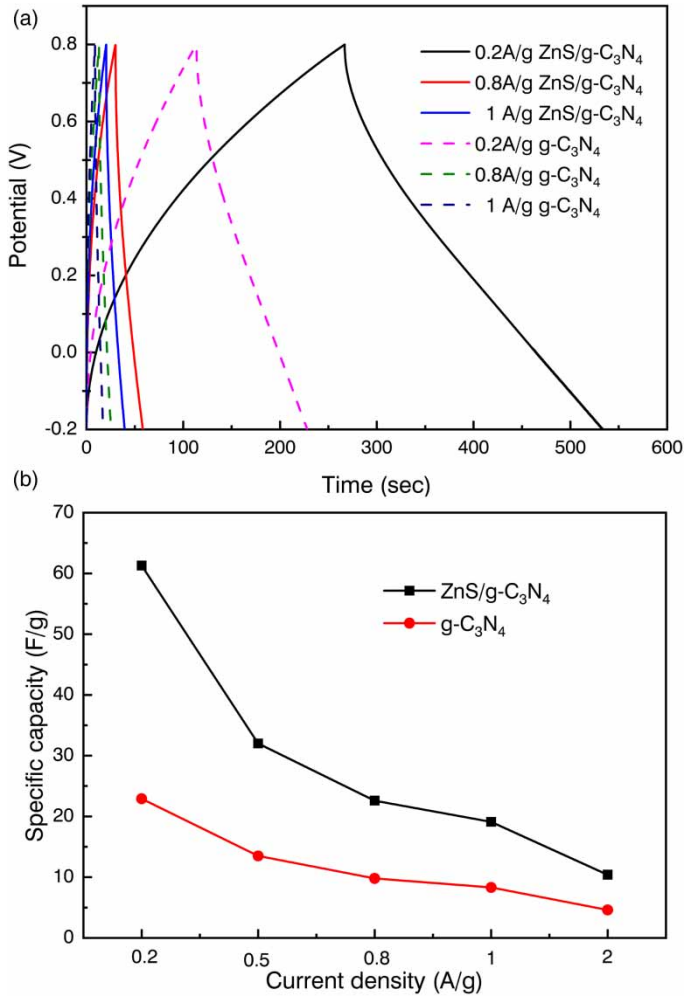

Figure 4 | GCD curves (a) and specific capacitances (b) of the g-C_3N_4 and ZnS/g-C_3N_4 electrodes at different current densities.

Table 2 | The electrosorption capacity of electrodes in different CDI modes

CDI mode	Capacity (mg/g)
g-C_3N_4//g-C_3N_4 (CDI)	4.61
ZnS/g-C_3N_4//ZnS/g-C_3N_4 (CDI)	8.38
g-C_3N_4//g-C_3N_4 (MCDI)	11.05
ZnS/g-C_3N_4//ZnS/g-C_3N_4 (MCDI)	27.65

reach the adsorption maximum, which can adsorb more ions than CDI cell (Broseus *et al.* 2009). During desorption, the ion concentration on the surface of the electrode plate of the MCDI cell is higher than that of the CDI cell. At the same time, a large number of ions in the CDI cell's solution suffer from the disadvantage of attraction to the side electrode, causing the ion desorption of the MCDI cell's electrode to be greater than that of the CDI cell. As a result, given the effect of membrane addition on treatment capacity and desalination, the MCDI mode is appropriate.

To further optimize the desalination performance, different voltages were applied to the ZnS/g-C_3N_4 electrode in MCDI mode. The amount of energy consumed during MCDI is directly proportional to the output voltage. At an initial NaCl concentration of 200 mg/L and a flow rate of 5 mL/min, the adsorption capacity gradually increased with the applied voltage (0.6–1.2 V), as shown in Figure 5(a) and 5(b). The electroabsorption capacity was 27.65 mg/g when the voltage was 1.2 V, and the desalination effect was relatively good. The electric field between the plates gets stronger as the plate voltage gets

higher, which speeds up the electrodes' desalination process. Therefore, MCDI may produce a higher desalination rate and realize better desalination results by increasing the electrode plate voltage as much as feasible without going above the electrode bilayer capacity load (Jande & Kim 2014; Li *et al.* 2019). As a result, in this experiment, the voltage of 1.2 V is advantageous for the MCDI desalination.

To investigate the desalination performance of ZnS/g-C_3N_4 composites at different inlet flow rates. At an initial NaCl concentration of 200 mg/L and an applied voltage of 1.2 V, different inlet flow rates (5, 10, 15, and 20 mL/min) were chosen for this experiment. Figure 5(c) and (d) shows the variation of the conductivity of the NaCl solution with time, as well as the calculated electrosorption capacity of the electrode after reaching adsorption equilibrium. The adsorption capacity decreases gradually as the inlet flow rate increases. The electrosorption capacity was 27.65 mg/g at a flow rate of 5 mL/min, and the desalination effect was relatively good. This could be due to the short retention time at high flow rates, which could reduce ion adsorption (Tang *et al.* 2015). Increased solution inlet flow rate may result in a shorter retention time of the raw aqueous solution in the flow channel, and the ions migrating to the electrode surface may not have been adequately adsorbed and stored in the double electric layer (Agartan *et al.* 2019). Alternatively, the ions adsorbed on the electrode surface are less than the impact force applied and flow out of the desalination unit with the solution, reducing the electrode adsorption capacity.

Figure 6 depicts the MCDI desalination of the ZnS/g-C_3N_4 composite electrode with varying initial NaCl concentration. At initial NaCl concentrations of 200, 400, and 600 mg/L, the adsorption amounts were 27.65, 50.26, and 65.34 mg/g,

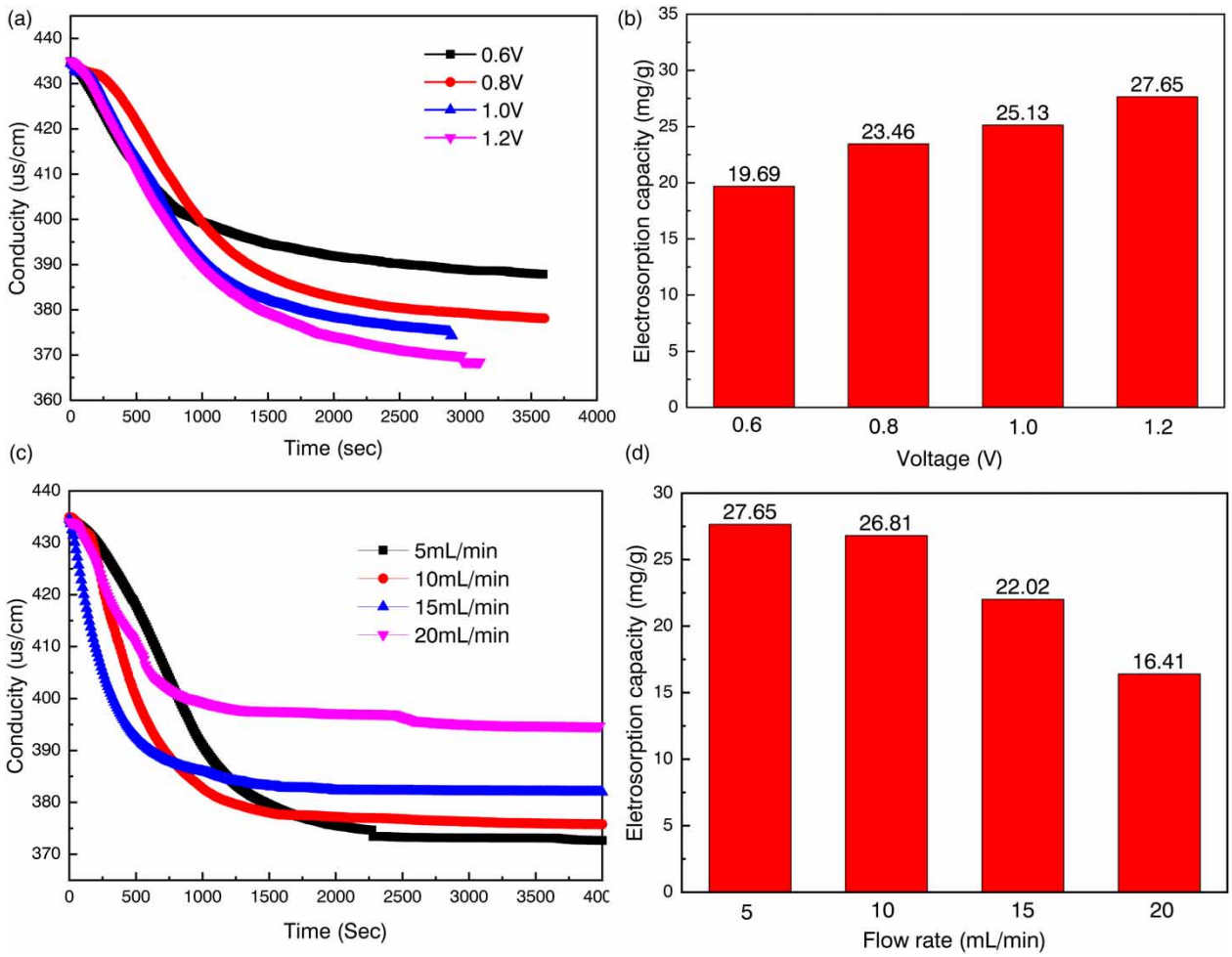

Figure 5 | Conductivity change during MCDI using ZnS/g-C_3N_4 electrodes under different voltages (a) and corresponding electrosorption capacities (b), and under flow rates (c), and corresponding electrosorption capacities (d).

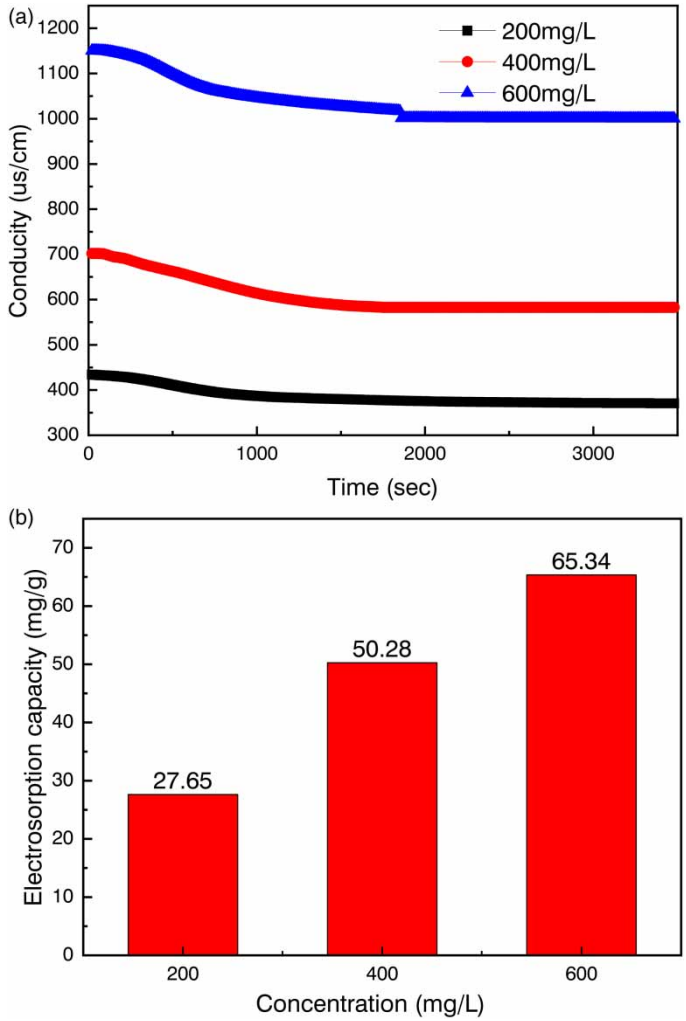

Figure 6 | Conductivity change during MCDI using ZnS/g-C_3N_4 electrodes in different initial NaCl concentrations (a) and corresponding electrosorption capacities (b).

respectively, at an operating voltage of 1.2 V and a flow rate of 5 mL/min. The desalination amount increased with the initial NaCl concentration, first rising and then reaching equilibrium. As the initial concentration increases, it leads to an increase in the bilayer capacitance and more salt ions come in contact with the active sites on the electrode material. Moreover, higher ion concentrations indicate a lower Ohmic loss of the solution, leading to a higher effective voltage between the electrodes and a subsequent increase in electrode adsorption (Zhao *et al.* 2013; Sakar *et al.* 2017). Furthermore, the conductivity of the solution increases, and the ion migration rate is subsequently accelerated, improving the electrode's desalination capacity.

CONCLUSION

In this study, a ZnS/g-C_3N_4 composite was successfully prepared by a one-step high-temperature calcination method and used as the main active material for electrodes in CDI desalination. SEM and TEM images revealed that spherical ZnS particles were evenly distributed on the layered structure of porous g-C_3N_4. N_2 adsorption–desorption tests and pore size distribution analysis demonstrated the ZnS/g-C_3N_4 composite had a larger specific surface area and suitable porous structure compared to g-C_3N_4 alone. Furthermore, ZnS/g-C_3N_4 exhibited favorable specific capacitance characteristics, relatively low resistance and high electrochemical stability. Notably, the ZnS/g-C_3N_4//ZnS/g-C_3N_4 (MCDI) electrodes showed a high adsorption capacity of 27.65 mg/g with an applied voltage of 1.2 V, a flow rate of 5 mL/min, and an initial NaCl concentration of 200 mg/L. When the initial concentration of NaCl increased to 400 and 600 mg/L, the adsorption capacity reached 50.26

and 65.34 mg/g, respectively. In summary, the ZnS/g-C_3N_4 composite electrodes could enable efficient desalination in MCDI systems.

ACKNOWLEDGEMENT

The research is financially supported by the fundamental research program of Shanxi Province (No. 20210302123051).

DATA AVAILABILITY STATEMENT

All relevant data are included in the paper or its Supplementary Information.

CONFLICT OF INTEREST

The authors declare there is no conflict.

REFERENCES

Agartan, L., Hayes-Oberst, B., Byles, B. W., Akuzum, B., Pomerantseva, E. & Kumbur, E. C. 2019 Influence of operating conditions and cathode parameters on desalination performance of hybrid CDI systems. *Desalination* **452**, 1–8.

Broseus, R., Cigana, J., Barbeau, B., Daines-Martinez, C. & Suty, H. 2009 Removal of total dissolved solids, nitrates and ammonium ions from drinking water using charge-barrier capacitive deionisation. *Desalination* **249** (1), 217–223.

Chung, H. J., Kim, J., Kim, D. I., Gwak, G. & Hong, S. 2020 Feasibility study of reverse osmosis-flow capacitive deionization (RO-FCDI) for energy-efficient desalination using seawater as the flow-electrode aqueous electrolyte. *Desalination* **479**, 114326.

Dlugolecki, P. & van der Wal, A. 2013 Energy recovery in membrane capacitive deionization. *Environ. Sci. Technol.* **47** (9), 4904–4910.

Du, X., Zhao, H., Zhang, Z., Lu, Y., Gao, C., Li, Z., Teng, Y., Zhao, L. & Swierczek, K. 2017 Core-shell structured ZnS-C nanoparticles with enhanced electrochemical properties for high-performance lithium-ion battery anodes. *Electrochim. Acta* **225**, 129–136.

Gong, A., Zhao, Y., He, M., Liang, B. & Li, K. 2021 High-performance desalination of three-dimensional nitrogen-doped carbon framework reinforced Prussian blue in capacitive deionization. *Desalination* **505**, 114997.

Guo, D., Song, X., Tan, L., Ma, H., Pang, H., Wang, X. & Zhang, L. 2018 Metal-organic framework template-Directed fabrication of well-aligned pentagon-like hollow transition-metal sulfides as the anode and cathode for high-performance asymmetric supercapacitors. *ACS Appl. Mater. Interfaces* **10** (49), 42621–42629.

Huang, Z. H., Yang, Z., Kang, F. & Inagaki, M. 2017 Carbon electrodes for capacitive deionization. *J. Mater. Chem. A* **5** (2), 470–496.

Jande, Y. A. C. & Kim, W. S. 2014 Modeling the capacitive deionization batch mode operation for desalination. *J. Ind. Eng. Chem.* **20** (5), 3356–3360.

Kavil, J., Anjana, P. M., Periyat, P. & Rakhi, R. B. 2018 One-pot synthesis of g-C3N4/MnO2 and g-C3N4/SnO2 hybrid nanocomposites for supercapacitor applications. *Sustain. Energ. Fuels* **2** (10), 2244–2251.

Leong, Z. Y., Lu, G. & Yang, H. Y. 2019 Three-dimensional graphene oxide and polyvinyl alcohol composites as structured activated carbons for capacitive desalination. *Desalination* **451**, 172–181.

Li, D., Wang, S., Wang, G., Li, C., Che, X., Wang, S., Zhang, Y. & Qiu, J. 2019 Facile fabrication of NiCoAl-Layered metal oxide/Graphene nanosheets for efficient capacitive deionization defluorination. *ACS Appl. Mater. Interfaces* **11** (34), 31200–31209.

Liao, G., Chen, S., Quan, X., Yu, H. & Zhao, H. 2012 Graphene oxide modified g-C3N4 hybrid with enhanced photocatalytic capability under visible light irradiation. *J. Mater. Chem.* **22** (6), 2721–2726.

Mohamed, S. K., Abuelhamd, M., Allam, N. K., Shahat, A., Ramadan, M. & Hassan, H. M. A. 2020 Eco-friendly facile synthesis of glucose-derived microporous carbon spheres electrodes with enhanced performance for water capacitive deionization. *Desalination* **477**, 114278.

Peng, Z., Zhang, D., Shi, L., Yan, T., Yuan, S., Li, H., Gao, R. & Fang, J. 2011 Comparative electroadsorption study of mesoporous carbon electrodes with various pore structures. *J. Phys. Chem. C* **115** (34), 17068–17076.

Porada, S., Zhao, R., van der Wal, A., Presser, V. & Biesheuvel, P. M. 2013 Review on the science and technology of water desalination by capacitive deionization. *Prog. Mater. Sci.* **58** (8), 1388–1442.

Sakar, H., Celik, I., Canbolat, C. B., Keskinler, B. & Karagunduz, A. 2017 Electro-sorption of ammonium by a modified membrane capacitive deionization unit. *Sep. Sci. Technol.* **52** (16), 2591–2599.

Sarma, B., Ray, R. S. & Misra, M. 2015 Charge storage in flower-like ZnS electrochemically deposited on TiO2 nanotube. *Mater. Lett.* **139**, 77–80.

Shiklomanov, I. A. 2000 Appraisal and assessment of world water resources. *Water Int.* **25** (1), 11–32.

Shiraz, H. G., Crispin, X. & Berggren, M. 2021 Transition metal sulfides for electrochemical hydrogen evolution. *Int. J. Hydrogen Energy* **46** (47), 24060–24077.

Sufiani, O., Elisadiki, J., Machunda, R. L. & Jande, Y. A. C. 2019 Modification strategies to enhance electrosorption performance of activated carbon electrodes for capacitive deionization applications. *J. Electroanal. Chem.* **848**, 113328.

Suss, M. E., Porada, S., Sun, X., Biesheuvel, P. M., Yoon, J. & Presser, V. 2015 Water desalination via capacitive deionization: What is it and what can we expect from it? *Energy Environ. Sci.* **8** (8), 2296–2319.

Tang, W., Kovalsky, P., He, D. & Waite, T. D. 2015 Fluoride and nitrate removal from brackish groundwaters by batch-mode capacitive deionization. *Water Res.* **84**, 342–349.

Thiagarajan, K., Bavani, T., Arunachalam, P., Lee, S. J., Theerthagiri, J., Madhavan, J., Pollet, B. G. & Choi, M. Y. 2020 Nanofiber nimoo4/g-C3N4 composite electrode materials for redox supercapacitor applications. *Nanomaterials* **10** (2), 392.

Torkamanzadeh, M., Wang, L., Zhang, Y., Budak, O., Srimuk, P. & Presser, V. 2020 MXene/Activated-carbon hybrid capacitive deionization for permselective ion removal at low and high salinity. *Acs Appl. Mater. Int.* **12** (23), 26013–26025.

Wang, S., Wang, G., Wu, T., Zhang, Y., Zhan, F., Wang, Y., Wang, J., Fu, Y. & Qiu, J. 2018 BCN nanosheets templated by g-C3N4 for high performance capacitive deionization. *J. Mater. Chem. A* **6** (30), 14644–14650.

Xie, D., Yuan, Y., Xiao, L., Cheng, F., Zhang, M., Fan, H. & Ge, X. 2018 Strain redistribution in metal-sulfide-composite anode for enhancing volumetric lithium storage. *ChemElectroChem* **5** (24), 3906–3912.

Xu, J., Zhang, W., Fan, H., Cheng, F., Su, D. & Wang, G. 2018 Promoting lithium polysulfide/sulfide redox kinetics by the catalyzing of zinc sulfide for high performance lithium-sulfur battery. *Nano Energy* **51**, 73–82.

Yan, T., Liu, J., Lei, H., Shi, L., An, Z., Park, H. S. & Zhang, D. 2018 Capacitive deionization of saline water using sandwich-like nitrogen-doped graphene composites via a self-assembling strategy. *Environ. Sci.-Nano* **5** (11), 2722–2730.

Zhang, J., Guo, F. & Wang, X. 2013 An optimized and general synthetic strategy for fabrication of polymeric carbon nitride nanoarchitectures. *Adv. Funct. Mater.* **23** (23), 3008–3014.

Zhao, Y., Wang, Y., Wang, R., Wu, Y., Xu, S. & Wang, J. 2013 Performance comparison and energy consumption analysis of capacitive deionization and membrane capacitive deionization processes. *Desalination* **324**, 127–133.

Zheng, Y., Liu, J., Liang, J., Jaroniec, M. & Qiao, S. Z. 2012 Graphitic carbon nitride materials: Controllable synthesis and applications in fuel cells and photocatalysis. *Energy Environ. Sci.* **5** (5), 6717–6731.

First received 7 July 2023; accepted in revised form 24 November 2023. Available online 7 December 2023